Measurement and Characterization of 28 GHz High-Speed Train Backhaul Channels in Rural Propagation Scenarios

Mathis Schmieder[1], Michael Peter[1], Ramez Askar[1], Ivan Komsic[1], Wilhelm Keusgen[1]
[1]Fraunhofer Heinrich Hertz Institute, Berlin, Germany, forename.surname@hhi.fraunhofer.de

***Abstract*—In this paper, the setup, scenario and first results of a measurement campaign on 28 GHz high-speed train backhaul channels are presented. The measurements were performed in a rural propagation scenario. Both large-scale measurements with a moving receiver and angle-resolved measurements with a static receiver at various positions were conducted to thoroughly characterize the environment. A novel virtual circular array antenna was employed to capture the angle-of-arrival information. The results show that the estimated angles correlate well with the environment. A path loss model for line of sight is parameterized and RMS delay and angle spreads are evaluated. The comparison with the 3GPP TR38.901 channel model parameters shows that the evaluated spreads are smaller that the 3GPP values but of the same order of magnitude as the values for the urban micro scenario.**

***Index Terms*—5G, channel sounding, mm-wave radio channel, direction of arrival, high-speed backhaul, measurement.**

I. Introduction

With the growing demand for 100+ Mbps user experience in order to support services like HD video streaming, and with the rapid growth of high-speed railway (HSR) services, it is mandatory to develop broadband communication systems for railways. Current technologies like the global system for mobile communications for railway (GSM-R) and even the long-term evolution for railway (LTE-R) only support low data rates between 172 kbps (GSM-R) and 50 Mbps (LTE-R). In order to fulfill the demand for higher data rates, a possibility is to use millimeter wave frequency bands like 28 GHz where higher bandwidths can be applied.

Ai et al. define 12 different HSR scenes in [1] with the *Viaduct* scene being the most common one. Several measurement campaigns (e.g. [2], [3]) have been conducted in such scenarios at sub 6 GHz frequencies. In Europe, the *Rural* scenario is much more common. While the WINNER D2a (rural moving network) channel model [4] provides a simple HSR scenario with only one LoS path in the 2 to 6 GHz frequency band, more work needs to be done to properly characterize realistic rural scenarios.

In this paper, we present channel measurements that have been performed at a freight depot with several train tracks, trees and buildings in order to develop a channel model for rural high-speed train scenarios. The channel was spatially captured both in a large-scale and small-scale manner using a wideband channel sounder setup operating at 28 GHz. The measurement results allow for characterizing the propagation environment by the path loss, delay-related channel parameters and the angle-of-arrival properties at the receiver side. Since the environment can be assumed as being mostly static, the findings from the measurements carried out at low speed can be transferred to high mobility scenarios by scaling the motion speed in the geometry-based stochastic channel model (GSCM). The results will be used to extend the QuaDRiGA [5] channel model.

In Section II the channel sounder hardware is introduced. Section III gives an overview of the measurement scenario, and first results obtained from the measurement campaign are described in IV.

II. Measurement Setup

The measurements were conducted using an advanced instrument-based highly flexible time-domain channel sounder setup. Fig. 1 gives a simplified overview of the hardware elements. An FPGA-based signal generator generates the sounding signal at an intermediate frequency of 3 GHz with a bandwidth of 933 MHz, corresponding to a temporal resolution of about 1.1 ns. A periodic Frank-Zadoff-Chu (FZC) sequence [6], [7] with perfect auto-correlation properties and therefore a frequency flat spectrum was employed to estimate the channel transfer function and impulse response. The IF signal is converted up to 28 GHz (λ = 10.71 mm) by mixing it with a local oscillator signal generated by a *Rohde & Schwarz SMB*. The RF signal is then fed through a power amplifier and transmitted using a vertically polarized omni-directional antenna.

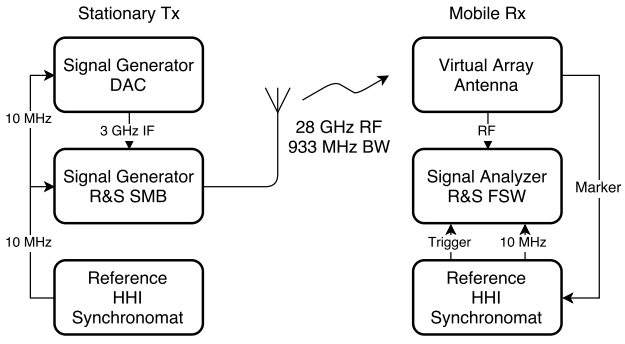

Fig. 1. Channel sounder setup used for measurements

At the receiver side, a virtual circular array antenna (VCA) as described in [8] is used. A *Rohde & Schwarz FSW* signal

analyzer captures the signal after it was fed through a low-noise amplifier and stores the baseband samples. The transmitter (Tx) and receiver (Rx) setup is synchronized using a high precision rubidium clock (Synchronomat from *Fraunhofer HHI*), which enables both sides to operate completely independent. It also enables coherent triggering of the receiver. Before the measurements, the system is calibrated on site via back-to-back measurement.

The virtual circular array has a diameter of 97.8 mm and the rotation speed was set to 625 rpm. One rotation, and therefore one complete measurement, takes 96 ms. A contiguous sampling of the virtual array was implemented by choosing a sequence duration of 96 μs, thus having 1000 virtual array elements equally distributed around the circular aperture. This results in a spacing between adjacent virtual array elements of 0.307 mm (0.0287 λ). The 96 μs sequence duration corresponds to a 89,568 element FZC sequence, yielding 49.5 dB processing gain. Each measurement was coherently triggered by the Synchronomat at the receiver. The received signal was sampled with a resolution of 16 bit. The omni-directional antennas had a gain of 0 dBi each and the average transmit power was 34 dBm, resulting in a maximum measurable path loss of about 140 dB. The important channel sounder parameters are summarized in Table I.

TABLE I
CHANNEL SOUNDER PARAMETERS

Type	Value
Carrier frequency	28 GHz
Transmit power	34 dBm
Sounding bandwidth	933 MHz
Sampling rate at Rx	1120 MHz
Sequence duration	96 µs
Temporal snapshot separation (Large Scale)	96 ms
Temporal snapshot separation (VCA)	96 µs

III. MEASUREMENT SCENARIO

The measurement campaign was performed at a freight depot in Elstal, near Berlin, Germany. The depot is located in a rural environment. Several tracks are running in parallel and are limited by trees on either side. A map of the measurement location is given in Fig. 3. Both Tx and Rx were placed on the beds of pick-up trucks. The amplifiers and antennas were mounted on tripods, allowing an easy adjustment of their height. At the Tx (Fig. 2, top), the antenna height was set to 5 m above ground. The Rx (Fig. 2, bottom) was placed at a height of 3 m. The positions of the antennas were chosen to represent a mobile backhaul scenario where a fixed base station is placed several meters higher than the mobile access point.

The Tx was placed at two fixed positions next to the train tracks as illustrated in Fig. 3. After Tx and Rx were calibrated using a back-to-back measurement, the Rx was moved along three paths, also illustrated in Fig. 3. For Rx Path 1, the Tx was placed at Tx Position 1, for Rx Paths 2 and 3, the Tx was placed at Tx Position 2. The minimal distance between Tx and Rx was 40 meter. Rx Paths 1 and 2 were mainly line-of-sight

Fig. 2. Transmitter and Receiver

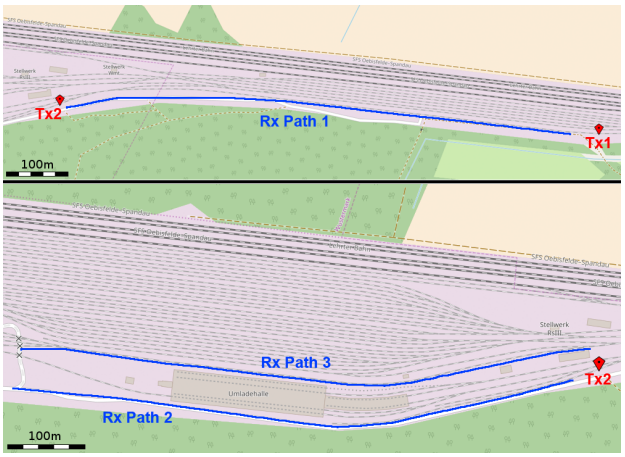

Fig. 3. Map of measurement location with Tx positions and Rx Paths

(LoS) while Rx Path 3 was mostly obstructed line-of-sight or non-line-of-sight (OLoS/NLoS).

In order to capture the large scale effects, the Rx was moved with a constant speed of 1.75 m/s along a path next to the train tracks. During each measurement run, which covered a distance of 850 m, 5000 CIR snapshots have been taken. This results in one CIR snapshot every 17.5 cm. The rotation of the virtual circular array antenna was disabled during these measurement runs, so that it acted as a simple vertical dipole antenna. For the direction-of-arrival (DoA) measurements, the receiver was placed at fixed positions every 20 m on each path. At each position, 1000 CIR snapshots were taken, corresponding to the 1000 virtual array elements.

IV. MEASUREMENT RESULTS

A. Power Delay Profile

As explained above, the channel sounder outputs a CIR every 17.5 cm on the large-scale measurements and 1000

CIRs every 20 m on the DoA measurements. An instantaneous power delay profile (IPDP) is calculated based on each CIR of the large scale measurements. An exemplary IPDP is illustrated in Fig. 4. The IPDPs are then analyzed for multipath components (MPCs). MPCs with a power less than the IPDP's median plus 13 dB are attributed to noise and discarded. This minimum power is denoted as *Absolute Threshold*. The dynamic range is defined as the distance between the maximum MPC and the absolute threshold. In Fig. 4, the identified MPCs are marked as *Evaluated Taps*.

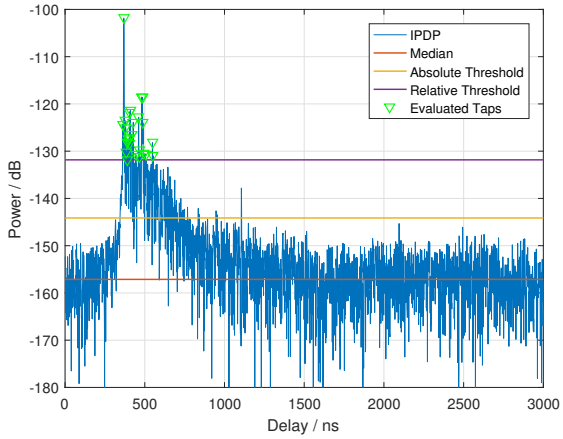

Fig. 4. Exemplary IPDP on Rx Path 1, distance 80 m

The output of the DoA measurements (1000 snapshots per position) are averaged, resulting in average power delay profiles (ADPDs). An exemplary APDP is illustrated in Fig. 5. Again, the APDPs are analyzed for MPCs, discarding components with a power lower than a relative threshold based on the strongest MPC.

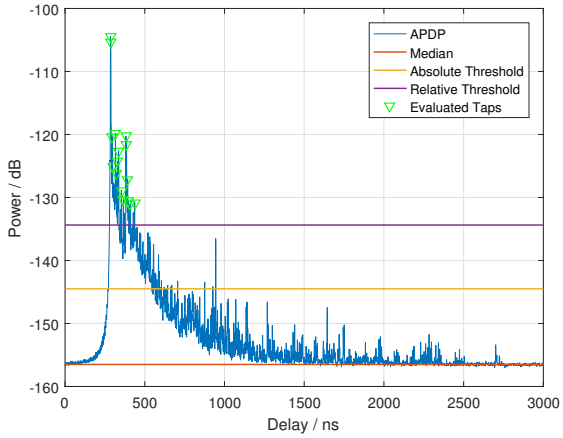

Fig. 5. Exemplary APDP on Rx Path 1, distance 80 m

B. Path Loss

The path loss was evaluated based on the results of the large scale measurements. In order to minimize the effects of small-scale fading, the cumulated powers of the identified MPCs were averaged over six consecutive IPDPs, corresponding to a path segment of 1.05 m. In Fig. 6, the evaluated path loss of all Rx paths are illustrated. As mentioned before, Rx Paths 1 and 2 were mainly LoS, while Rx Path 3 was mainly NLoS/OLoS due to buildings between Tx and Rx. Transitions from LoS to NLoS due to bends in the tree lined paths can be found at 565 m in Rx Path 1 and at 330 m in Rx Path 2 and lead to an increase in the path loss of about 15 dB. This is confirmed by the results of Rx Path 3, where a transition from NLoS to LoS occurs at 183 m, which results in a decrease in the path loss of about 15 dB. Noticeable fluctuations in the path loss due to ground reflection effects can be seen the results of Rx Path 1 between 300 and 550 m.

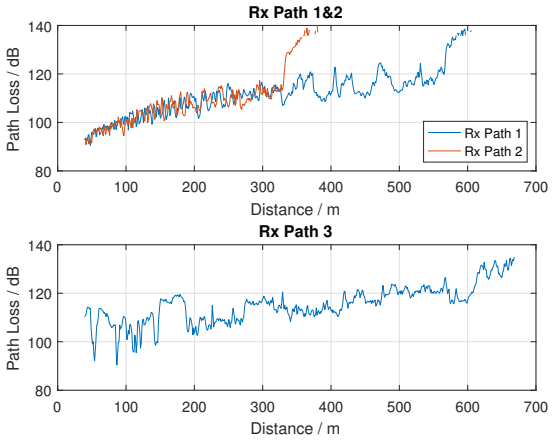

Fig. 6. Path losses of all Rx paths

Based on the results of Rx Paths 1 and 2 in pure LoS conditions, a floating intercept (FI) and a fixed reference (FR) [9], [10] path loss model were parameterized. In Fig. 7, a scatter plot of the data samples and the resulting linear least squares fits are illustrated. Both models are very close to the free space path loss. In Table II, the resulting path loss coefficients are given, where d_0 is the reference distance, and $\bar{L}_{PL}(d_0)$ is the mean path loss at that distance. For the FI model, both $\bar{L}_{PL}(d_0)$ and n were obtained through the fit, while for the FR model, $\bar{L}_{PL}(d_0)$ was set to be equal to the free space path loss.

TABLE II
PATH LOSS PARAMETERS

	d_0	n	$\bar{L}_{PL}(d_0)$	σ
FI Model	1 m	2.27	55.7 dB	2.8
FR Model	1 m	2.03	61.4 dB	2.8

C. RMS Delay Spread

The root mean square (RMS) delay spread (DS) was calculated based on the IPDPs of Rx Paths 1 and 2 in LoS condition. A relative evaluation threshold of either 20 or 30 dB was applied, meaning that MPCs below of -20 or -30 dB relative to the strongest MPC are discarded. Only IPDPs with a dynamic range exceeding the relative threshold were taken into account. The results have shown that a relative threshold of 20

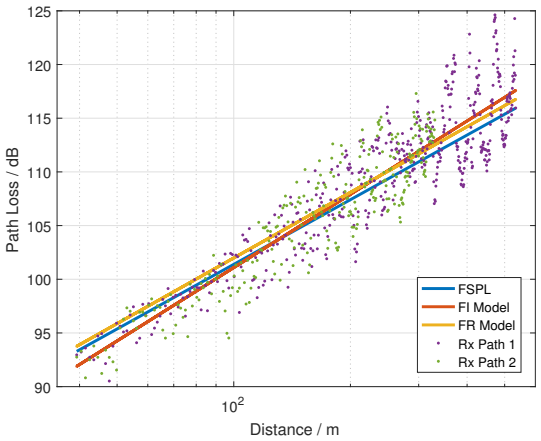

Fig. 7. Line-of-sight path loss and linear regressions

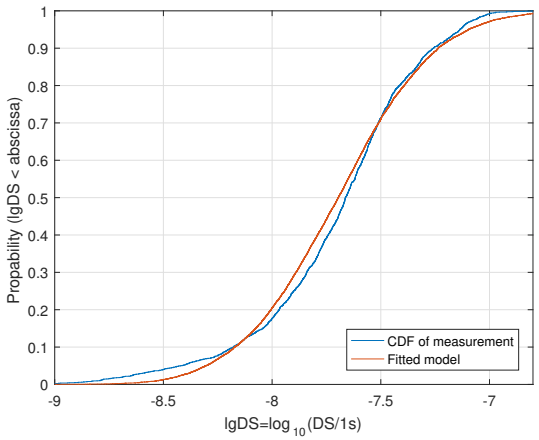

Fig. 9. CDF of RMS delay spread, logarithmic scaling

dB leads to very few MPCs, and therefore reduces the delay spread unnaturally. Fig. 8 shows the cumulative distribution functions (CDF) of the RMS delay spread with 20 and 30 dB threshold, exhibiting much lower values for 20 dB. In the present case, a relative threshold of 30 dB is more appropriate.

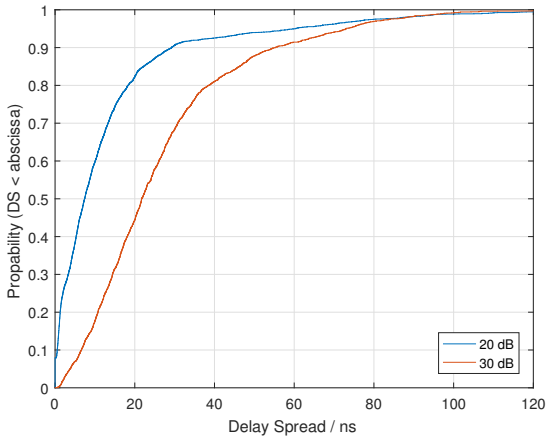

Fig. 8. CDF of RMS delay spread, linear scaling

To be in line with 3GPP channel modeling [11], the RMS delay spread was also evaluated on a logarithmic scale. In Fig. 9, the CDF of the RMS delay spread with a threshold of 30 dB is illustrated together with the fitted model. The statistical parameters are given in Table III together with the 3GPP TR 38.901 [11] channel model values for the *Urban Micro* (UMi) and *Urban Macro* (UMa) LoS scenarios. The results of the evaluation with a relative threshold of 20 dB are not suitable for model fitting on a logarithmic scale due to the frequent occurance of delay spreads of 0 ns.

D. RMS Azimuth/Zenith Angle Spread of Arrival

The RMS angle spreads of arrival were calculated based on the DoA measurements using the virtual circular array antenna. As for the previous parameters, only the LoS parts of Rx Paths

TABLE III
STATISTICAL PARAMETERS OF THE RMS DELAY SPREAD (DS): MEAN μ_{DS}, MEDIAN m_{DS}, STANDARD DEVIATION σ_{DS}, AND 95%-QUANTILE $Q_{DS,0.95}$

Measurement			Comparative values	
Parameter	20 dB th.	30 dB th.	3GPP UMi	3GPP UMa
μ_{DS} (ns)	13.6	27.1	-	-
m_{DS} (ns)	7.41	21.7	-	-
σ (ns)	20.2	21.1	-	-
$Q_{DS,0.95}$ (ns)	59.9	73.0	-	-
μ_{lgDS}	-	-7.70	-7.49	-7.09
σ_{lgDS}	-	0.37	0.38	0.66

1 and 2 were used for the calculation. In Fig. 10, the CDF of the RMS azimuth (ASA) and zenith (ZSA) angle spreads of arrival are illustrated. It can clearly be seen that the ASA is much higher than the ZSA. The statistical parameters are given in Table IV, again together with the 3GPP TR 38.901 UMi and UMa LoS values.

TABLE IV
STATISTICAL PARAMETERS OF THE RMS ANGLE SPREADS OF ARRIVAL (ASA/ZSA): MEAN $\mu_{ASA/ZSA}$, MEDIAN $m_{ASA/ZSA}$, STANDARD DEVIATION $\sigma_{ASA/ZSA}$, AND 95%-QUANTILE $Q_{ASA/ZSA,0.95}$

Measurement			Comparative values	
Parameter	ASA	ZSA	3GPP UMi	3GPP-UMa
$\mu_{ASA/ZSA}$ (°)	27.8	7.53	-	-
$m_{ASA/ZSA}$(°)	28.4	7.10	-	-
$\sigma_{ASA/ZSA}$ (°)	12.3	3.47	-	-
$Q_{ASA/ZSA,0.95}$ (°)	40.6	12.3	-	-
μ_{lgASA}	1.42		1.61	1.81
σ_{lgZSA}	0.19		0.30	0.20
μ_{lgZSA}	0.084		0.058	0.095
σ_{lgZSA}	0.21		0.28	0.16

E. Exemplary DoA Result

As an exemplary result for the direction of arrival measurements, the estimated power angular spectrum (PAS) in azimuth was calculated. A position on Rx Path 3 was chosen because the buildings on that path lead to reflections and therefore a wider angle spread. The estimated PAS is illustrated in Fig. 11 with the corresponding Rx and Tx positions on an

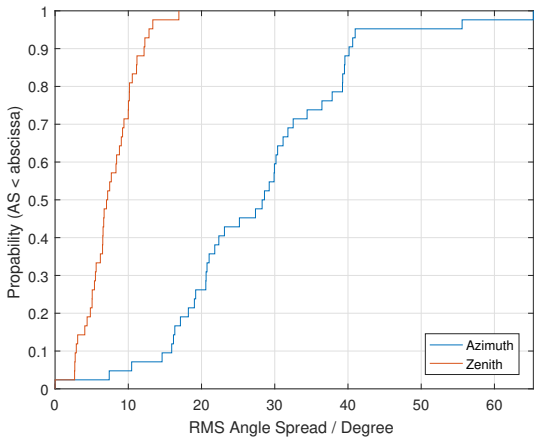

Fig. 10. CDF of angle spread

aerial picture in Fig. 12. Both the LoS path and strong multipath components due to reflections on the buildings can be identified.

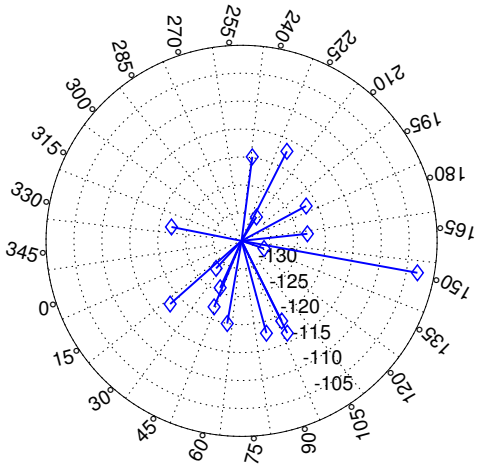

Fig. 11. Estimated PAS, Azimuth Angle (dBm)

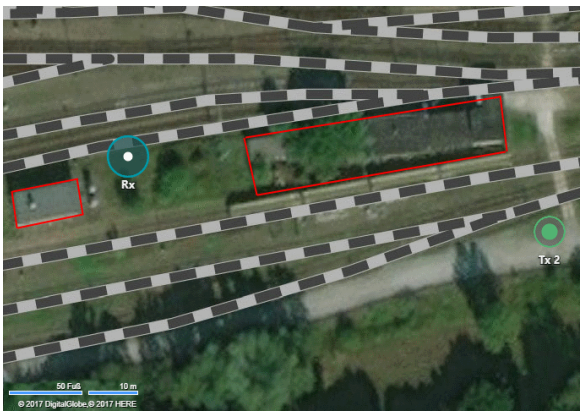

Fig. 12. Rx and Tx position for exemplary result

V. Conclusion

In this paper, we presented the setup, scenario and first results of a measurement campaign on 28 GHz high-speed train backhaul channels. In was conducted in a rural propagation scenario, comprising both large-scale and angle-resolved measurements. For the direction-of-arrival measurements, a novel virtual circular array antenna was employed and the results have shown that the estimated angles correlate well with environmental scatterers. A path loss model has been parameterized which is very close to the free space path loss. The RMS delay and angle spreads are smaller, but of the same order of magnitude as the values of the 3GPP TR 38.901 channel model in the UMi and UMa LoS scenarios. The results will be integrated into the QuaDRiGa [5] channel model.

Acknowledgment

The research leading to these results received funding from the European Commission H2020 programme under grant agreement no. 723247 (5GCHAMPION) and the Korea Ministry of Science, ICT and Future Planning (Grant B0115-16-0001).

References

[1] B. Ai, R. He, Z. Zhong, K. Guan, B. Chen, P. Liu, and Y. Li, "Radio wave propagation scene partitioning for high-speed rails," *International Journal of Antennas and Propagation*, vol. 2012, 2012.

[2] L. Liu, C. Tao, J. Qiu, H. Chen, L. Yu, W. Dong, and Y. Yuan, "Position-based modeling for wireless channel on high-speed railway under a viaduct at 2.35 GHz," *IEEE Journal on Selected Areas in Communications*, vol. 30, no. 4, pp. 834–845, 2012.

[3] R. He, Z. Zhong, B. Ai, G. Wang, J. Ding, and A. F. Molisch, "Measurements and analysis of propagation channels in high-speed railway viaducts," *IEEE Transactions on Wireless Communications*, vol. 12, no. 2, pp. 794–805, 2013.

[4] J. Meinilä, P. Kyösti, T. Jämsä, and L. Hentilä, "WINNER II channel models," *Radio Technologies and Concepts for IMT-Advanced*, pp. 39–92, 2009.

[5] S. Jaeckel, L. Raschkowski, K. Borner, and L. Thiele, "Quadriga: A 3-D multi-cell channel model with time evolution for enabling virtual field trials," *IEEE Transactions on Antennas and Propagation*, vol. 62, no. 6, pp. 3242–3256, 2014.

[6] D. Chu, "Polyphase codes with good periodic correlation properties (corresp.)," *IEEE Transactions on Information Theory*, vol. 18, no. 4, pp. 531–532, 1972.

[7] R. Frank, "Comments on "Polyphase codes with good periodic correlation properties" by Chu, David C." *IEEE Transactions on Information Theory*, vol. 19, no. 2, pp. 244–244, 1973.

[8] H.-A. Nguyen, W. Keusgen, and T. Eichler, "Instantaneous direction of arrival measurements in mobile radio channels using virtual circular array antennas," in *Globecom Workshops (GC Wkshps), 2016 IEEE*. IEEE, 2016, pp. 1–7.

[9] K. Haneda, N. Omaki, T. Imai, L. Raschkowski, M. Peter, and A. Roivainen, "Frequency-agile pathloss models for urban street canyons," *IEEE Transactions on Antennas and Propagation*, vol. 64, no. 5, pp. 1941–1951, 2016.

[10] S. Sun, T. S. Rappaport, S. Rangan, T. A. Thomas, A. Ghosh, I. Z. Kovacs, I. Rodriguez, O. Koymen, A. Partyka, and J. Jarvelainen, "Propagation path loss models for 5G urban micro-and macro-cellular scenarios," in *Vehicular Technology Conference (VTC Spring), 2016 IEEE 83rd*. IEEE, 2016, pp. 1–6.

[11] 3rd Generation Partnership Project (3GPP), "3GPP TR 38.901 V14.2.0: Study on channel model for frequencies from 0.5 to 100 GHz," 3GPP, Tech. Rep., September 2017.